MSS-RSC

Modular Stone Standard
Robotic Stone Construction

A Mechanical Interface Protocol for
Deterministic Modular Stone Assembly

Status:	Open Academic Protocol (Initial Public Release)
Date:	February 2026
License:	CC-BY-SA 4.0
Intended use:	Replication, validation, extension

This document defines mechanical interface classes, dimensional tolerances, structural performance targets, and a digital-to-physical workflow for compression-dominant modular stone assemblies produced via robotic subtractive fabrication.

It does not prescribe architectural form. It prescribes mechanical grammar.

Contents

Abstract

Stone possesses compressive strength ranging from 60–250 MPa, high chemical stability, and demonstrated service lives exceeding 200 years, yet its role in contemporary construction is predominantly ornamental. The barriers are systemic: inconsistent joint geometry, labor-dependent tolerance correction, non-deterministic assembly logic, and the absence of a standardized mechanical interface linking robotic fabrication precision to structural performance guarantees.

This paper presents **MSS-RSC**, a normative mechanical interface protocol for compression-dominant modular stone systems produced via robotic subtractive fabrication. The protocol defines four interface classes—kinematic seating geometry, shear-transfer keys, dowel indexing systems, and controlled bedding zones—each specified with dimensional tolerances, performance equations, and verification procedures. The framework formally separates expressive architectural geometry from invariant structural interfaces, enabling parametric surface variation while preserving deterministic load-path behavior.

A digital-to-physical workflow is specified, including parametric segmentation, toolpath generation with cutter-wear compensation (± 0.5 mm structural tolerance), in-process structured-light verification, and Monte Carlo tolerance propagation modeling. Finite element analysis of a representative 48-module wall assembly demonstrates compressive stress uniformity within 8% across bearing interfaces and shear-key capacity exceeding $1.5\times$ the design lateral load under EN 1996-1-1 assumptions. Sensitivity analysis indicates robustness to angular misalignment up to $0.3°$.

MSS-RSC is released as an open protocol for replication, experimental validation, and community extension.

Keywords: robotic stone fabrication, modular construction, mechanical interface, digital fabrication, compression-dominant assembly, tolerance management

1 Introduction

1.1 Context

Stone has served as the primary structural material in compression-dominant architecture for millennia. Its material properties—compressive strength of 60–250 MPa across common building grades, fire resistance, negligible maintenance, and service lives routinely exceeding 100 years—make it one of the most efficient load-bearing materials for gravity-dominant structures [1, 2].

Despite these advantages, structural stone use has declined since the mid-twentieth century. The causes are systemic rather than material:

1. **Labor intensity.** Traditional ashlar masonry requires skilled masons at throughputs 5–10× lower than precast concrete operations.
2. **Geometric inconsistency.** Manual dressing produces joint surfaces with positional variability exceeding ±3 mm, requiring thick mortar beds (>5 mm) that introduce compliance and long-term creep.
3. **Tolerance unpredictability.** Without machined datum surfaces, cumulative stack-up deviations in multi-course assemblies are poorly bounded, complicating both structural analysis and crane logistics.
4. **Workflow fragmentation.** No standardized pipeline links quarry selection, robotic machining, dimensional verification, and site assembly into a coherent system.

Robotic subtractive fabrication resolves the geometric precision problem—achieving interface tolerances of ±0.5 mm on architectural-scale modules—but fabrication capability alone does not constitute a construction system. A standardized mechanical interface protocol is the missing component.

1.2 Prior Art and Gap

Significant research has addressed individual elements of robotic stone construction. Gramazio Kohler Research and ETH Zurich demonstrated robotic masonry placement with millimeter-level accuracy [3, 4]. Fallacara advanced the stereotomic geometry of interlocking stone [5]. Block and Ochsendorf developed compression-only vault design via discrete element methods [6]. Rippmann et al. demonstrated full-scale unreinforced stone vaults [7]. Ongoing research at multiple institutions has produced experimental digital stone prototypes at demonstrator scale.

However, no prior work proposes a *unified, normative protocol* that simultaneously specifies:

- Deterministic kinematic seating with quantified tolerance envelopes
- Shear-transfer keying with codified capacity equations
- Dowel-indexed alignment with pull-out design values
- Controlled bedding compliance with creep and drainage provisions
- Stochastic tolerance propagation integrated into assembly sequencing

MSS-RSC addresses this gap.

1.3 Contribution

This protocol makes three contributions:

1. A mechanical interface taxonomy that formally separates expressive surface geometry from invariant structural interfaces, specified as numbered normative requirements.
2. A digital-to-physical workflow with quantified tolerance targets at each stage.
3. Preliminary structural validation via finite element analysis, with results sufficient to bound the performance envelope pending experimental confirmation.

2 Protocol Scope and Non-Goals

2.1 Scope

MSS-RSC applies to:

- Compression-dominant modular stone assemblies (walls, piers, vaults, buttresses)
- Modules produced by robotic subtractive fabrication (CNC or 6-axis)
- Individual module mass $\leq 1500\,\text{kg}$
- Structural wall, pier, and façade systems
- Assembly under tower crane or equivalent lifting with positional accuracy $\pm 5\,\text{mm}$

2.2 Non-Goals

This protocol does not address:

- Reinforced stone with embedded steel cages or post-tensioning
- Adhesive-dependent thin veneers ($<30\,\text{mm}$ thickness)
- Purely ornamental carving without structural function
- Tensile-dominant or bending-dominant stone structures
- Seismic design (reserved for future protocol extension)

3 Governing Design Principle

The protocol is governed by a single axiom:

MSS-RSC-REQ-01 : Separation of Geometric Domains
Expressive architectural surface geometry shall be topologically and metrologically independent from structural interface geometry. Fabrication deviations on expressive surfaces shall have no first-order effect on load-path behavior, assembly sequencing, or cumulative tolerance propagation.

This separation permits non-repeating parametric surfaces on visible faces while structural interfaces remain standardized, repeatable, and mechanically deterministic. Figure 1 illustrates the principle.

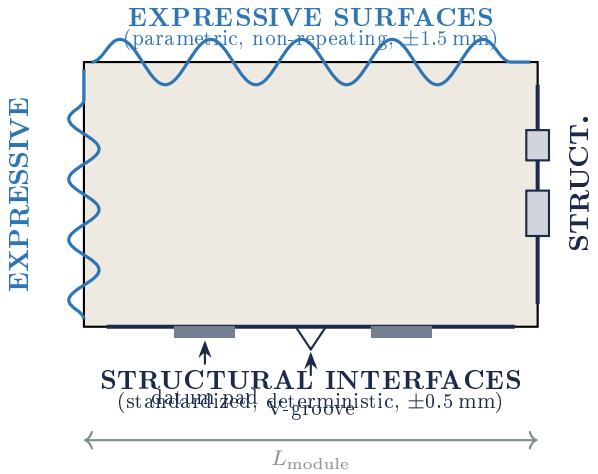

Figure 1. Domain separation principle. Expressive surfaces (blue, variable) are geometrically independent from structural interfaces (dark, invariant). Interface tolerances are 3× tighter than expressive tolerances.

4 Mechanical Interface Specification

4.1 Material Properties

Table 1 provides reference properties for common building stones. All subsequent calculations use conservative lower-bound values.

Table 1. Reference material properties for common building stones.

Property	Limestone	Granite	Unit
Compressive strength $f_{c,k}$	60–120	130–250	MPa
Elastic modulus E	20–60	40–70	GPa
Flexural tensile strength f_t	3–8	7–15	MPa
Poisson's ratio ν	0.20–0.30	0.20–0.27	—
Density ρ	2200–2700	2600–2800	kg/m^3
Friction coefficient μ (dressed)	0.60–0.75	0.65–0.80	—
Thermal expansion α	4–8	7–9	μm/(m·K)

4.2 Interface Class 1: Kinematic Seating Geometry

MSS-RSC-REQ-02 : Kinematic Constraint
Each module shall rest on a three-point kinematic constraint system providing five constrained degrees of freedom. The unconstrained DOF is vertical compression under gravity load. Placement under crane tolerance of ±5 mm shall be accommodated by lead-in chamfers.

4.2.1 Component Specification

1. **Primary Datum Pad.** Precision-machined flat zone, diameter ≥ 40 mm, surface flatness ≤ 0.1 mm, positional tolerance ±0.5 mm. Provides principal bearing surface and vertical reference.

2. **Secondary V-Groove.** Linear groove constraining one horizontal translational DOF. Groove angle 90°, depth 5–8 mm. Provides rotational reference about the vertical axis.
3. **Tertiary Stop.** Point or short-edge contact (≤ 20 mm) constraining the remaining horizontal DOF.
4. **Lead-in Chamfers.** 45° chamfers, 3–5 mm, on all seating edges. Permits guided placement within the crane positional envelope.

4.2.2 Bearing Stress

The bearing stress at kinematic seating interfaces shall satisfy:

$$\sigma_{\text{bearing}} = \frac{F_z}{A_{\text{eff}}} \leq \frac{f_{c,k}}{\gamma_M} \tag{1}$$

where F_z is the vertical load, A_{eff} is the effective bearing area (sum of datum pad contact zones), $f_{c,k}$ is the characteristic compressive strength, and γ_M is the material partial safety factor per EN 1996-1-1.

MSS-RSC-REQ-03 : Stress Uniformity
The ratio of peak bearing stress to mean bearing stress across kinematic contact zones shall not exceed 1.35: $\sigma_{\max}/\sigma_{\text{mean}} \leq 1.35$.

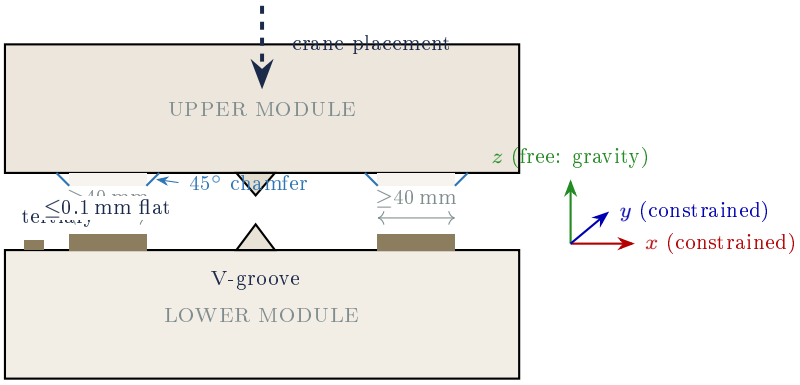

Figure 2. Kinematic seating geometry. Upper module descends onto three-point constraint: two datum pads, one V-groove, and a tertiary stop. Lead-in chamfers accommodate ±5 mm crane tolerance.

4.3 Interface Class 2: Shear-Transfer Keys

MSS-RSC-REQ-04 : Shear Resistance
Horizontal load transfer between modules shall be provided by interlocking shear keys. The design shear resistance V_{Rd} shall exceed the design shear force V_{Ed} by a factor ≥ 1.5.

4.3.1 Type A: Tongue-and-Groove

Rectangular cross-section keys running parallel to the wall face. Key depth $d_k = 8$–12 mm, width $w_k = 15$–25 mm, root radius $r \geq 2$ mm to limit stress concentration. Clearance gap $c = 0.5$–1.0 mm per side.

4.3.2 Type B: Spline Channel

Curved or multi-directional keying channels accepting a stone or GFRP spline insert. Provides bi-directional shear resistance for curved-plan assemblies. Spline cross-section: trapezoidal, 10–15 mm depth, 20–30 mm width.

4.3.3 Shear Capacity

The design shear resistance of a keyed joint follows the Mohr–Coulomb model adapted for keyed masonry joints per EN 1996-1-1 §3.6.2:

$$V_{Rd} = \frac{n_k \, A_k \, f_{vk0}}{\gamma_M} + \mu \, N_{Ed} \tag{2}$$

where n_k is the number of active keys, A_k is the key shear area, f_{vk0} is the characteristic initial shear strength, μ is the friction coefficient, and N_{Ed} is the design compressive force on the joint.

The following simplifying assumptions apply: (i) the governing failure mode is shear fracture at the key root; (ii) no prying action is considered at the key–module interface; (iii) stress distribution across the key root is assumed uniform; and (iv) tension cracking in the surrounding stone matrix is not modeled within the linear elastic framework. These assumptions are conservative for compression-dominant assemblies but would require nonlinear discrete element or fracture mechanics validation under combined or cyclic loading.

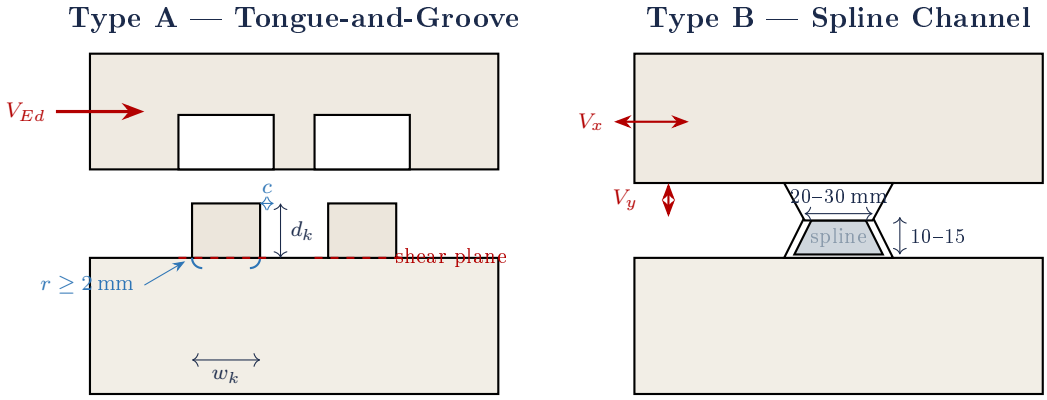

Figure 3. Shear key typology. Left: Type A tongue-and-groove for in-plane shear. Right: Type B spline channel for bi-directional shear in curved assemblies. Dashed lines indicate shear failure planes.

4.4 Interface Class 3: Dowel Indexing System

Dowels serve two functions: alignment indexing during placement, and uplift resistance under net-tension loading (e.g., wind suction on façade panels). They are *not* primary structural elements under normal gravity loading.

MSS-RSC-REQ-05 : Dowel Specification

Dowels shall be 316L stainless steel (ϕ12–16 mm) or GFRP (ϕ16–20 mm). Socket diameter: $\phi + 1.0$ mm. Positional tolerance: ± 0.5 mm. Embedment depth: $\geq 2.5\phi$ per side. Grout: thixotropic epoxy or cementitious adhesive.

4.4.1 Pull-Out Capacity

$$F_{\text{pullout}} = \pi \, \phi \, L_{\text{embed}} \, f_{\text{bond}} \tag{3}$$

where ϕ is the dowel diameter, L_{embed} is the embedment length, and f_{bond} is the design bond strength of the grout-to-stone interface (typically 1.5–3.0 MPa for epoxy-grouted limestone).

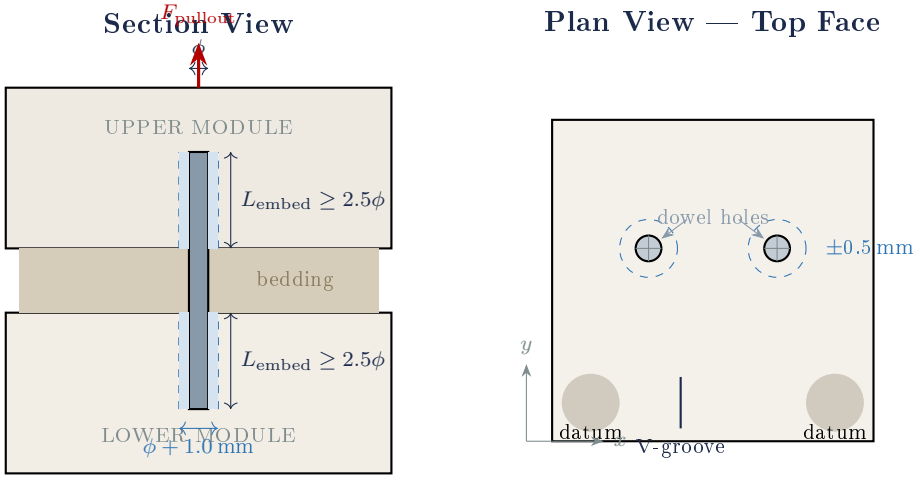

Figure 4. Dowel indexing system. Left: vertical section showing dowel, grout annulus, and embedment in upper and lower modules. Right: plan view of module top face showing dowel positions relative to kinematic datum features, with ±0.5 mm positional tolerance zones (dashed circles).

4.5 Interface Class 4: Controlled Bedding Zones

The bedding interface accommodates residual machining deviations, thermal movement, and construction tolerances through a controlled compliance layer.

MSS-RSC-REQ-06 : Bedding Compliance
The bedding zone shall provide a defined tolerance absorption envelope of ±1.5 mm and shall integrate drainage and capillary break geometry. Bedding material shall have a compressive modulus E_{bed} in the range 5–15 GPa.

4.5.1 Bedding Options

1. **Thin-bed mortar:** 1–3 mm polymer-modified mortar, $E_{\text{bed}} \approx$ 5–15 GPa. Suitable for permanent structural joints.
2. **Calibrated shims:** Polymer or lead shims at kinematic datum points, providing precise height adjustment within the ±1.5 mm envelope. Suitable for dry-stack and demountable assemblies.

4.5.2 Thermal Movement

Thermal expansion at the joint interface:

$$\Delta L = \alpha \, L \, \Delta T \tag{4}$$

where α is the coefficient of thermal expansion (see Table 1), L is the module dimension, and ΔT is the temperature differential. For a 600 mm limestone module with $\alpha = 6\,\mu\text{m}/(\text{m}\cdot\text{K})$ and $\Delta T = 40$ K, the expansion is $\Delta L = 0.14$ mm—well within the joint tolerance.

4.5.3 Creep Provisions

Mortar creep under sustained compressive load shall be accounted for in long-term deviation modeling. Preliminary design assumption: creep coefficient $\varphi = 1.5$–2.5 at 10 years, consistent with polymer-modified cementitious mortars. Experimental characterization is required (see §10).

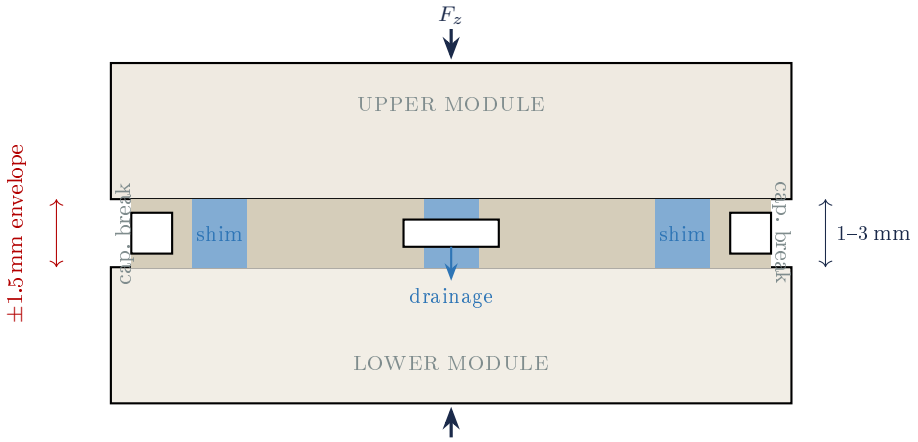

Figure 5. Controlled bedding zone (section). Calibrated shims at three kinematic datum points provide height adjustment. Central drainage channel and edge capillary breaks prevent moisture retention. Mortar fills remaining area for load distribution.

5 Digital-to-Physical Workflow

5.1 Parametric Segmentation

A global building geometry is decomposed into discrete modules subject to simultaneous constraints:

$$\text{minimize} \sum_i |m_i - m_{\text{target}}| \quad \text{s.t.} \quad m_i \le m_{\max}, \;\; L_i \le L_{\text{reach}}, \;\; t_i \ge t_{\min} \tag{5}$$

where m_i is the mass of module i (target $\le 1500\,\text{kg}$), L_i is the maximum extent from fixturing datum ($\le 2.5\,\text{m}$ for typical 6-axis reach), and t_i is the minimum structural wall thickness. Additional constraints include stone grain direction relative to principal stress trajectories and quarry block yield optimization.

5.2 Toolpath Generation

Each module's geometry is decomposed into two machining domains:

- **Structural interfaces:** ±0.5 mm tolerance, diamond-segment finishing.
- **Expressive surfaces:** ±1.5 mm tolerance, adaptive roughing.

Cutter-wear compensation is applied in real-time:

$$r_{\text{eff}}(t) = r_{\text{nominal}} - \alpha\, t_{\text{cut}} \tag{6}$$

where α is the empirical wear rate (approximately $0.02\,\text{mm/hour}$ for diamond-segment tools on granite).

5.3 In-Process Verification

Following machining, each module is scanned using structured-light metrology:

- Point spacing $\leq 0.5\,\text{mm}$
- Measurement uncertainty $\pm 0.05\,\text{mm}$
- Registration to nominal CAD model

Interface surfaces exceeding the $\pm 0.5\,\text{mm}$ tolerance trigger re-machining or reclassification into a tolerance-compensated assembly position.

5.4 Piece-Level Metadata

Each module carries:

1. Machine-readable Data Matrix (engraved on non-visible interface surface)
2. Human-readable UID on bedding face
3. Orientation arrow indicating installation axis

The UID links to a digital record: as-designed geometry, as-built scan, deviation map, material traceability, assembly position, and adjacent-module UIDs.

5.5 Tolerance Propagation Modeling

Monte Carlo simulation models the stochastic propagation of machining deviations through the assembly:

$$\Delta z_n = \sum_{i=1}^{n} \varepsilon_i, \qquad \varepsilon_i \sim \mathcal{N}(0,\, \sigma^2_{\text{mach}}) \tag{7}$$

where Δz_n is the cumulative vertical deviation at course n and $\sigma_{\text{mach}} \leq 0.25\,\text{mm}$.

Note: This model assumes independence between successive joint deviations. Systematic biases—such as consistent tool deflection under load or thermal drift of the robot arm—would violate this assumption and must be characterized empirically. If systematic bias μ_{bias} is detected, Eq. 7 becomes $\Delta z_n = n\mu_{\text{bias}} + \sum \varepsilon_i$, making bias correction a priority calibration target.

The simulation outputs a probability distribution of cumulative deviation at each course, enabling pre-planned error-compensation zones (thicker bedding or shimming).

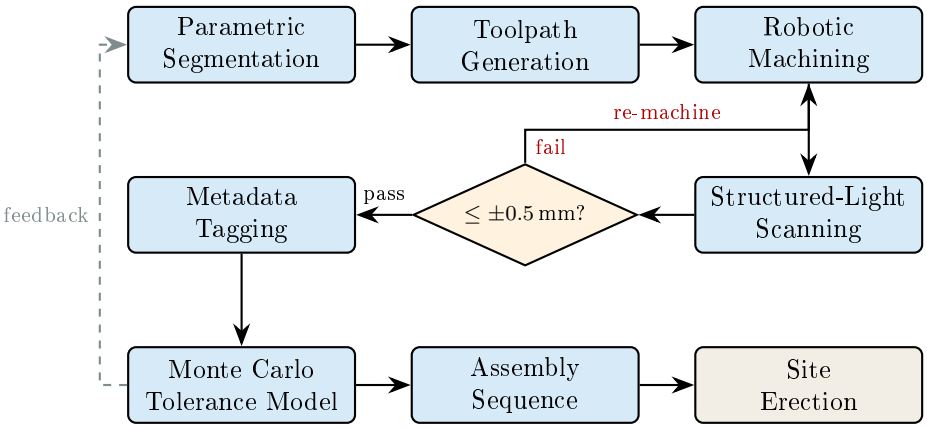

Figure 6. Digital-to-physical workflow. Each module passes through segmentation, machining, verification (with re-machining loop), metadata tagging, and tolerance simulation before entering the assembly sequence.

6 Structural Validation (Reference Implementation)

6.1 Reference Assembly

A straight wall is modeled as the reference assembly:

- Height: 3.0 m Thickness: 0.4 m Length: 6.0 m
- 48 modules (6 courses × 8 modules) in running bond
- Boundary conditions: fixed base, free top
- Vertical load: 200 kN/m uniformly distributed
- Lateral load: 1.5 kN/m^2 wind pressure per EN 1991-1-4
- Material: limestone, lower-bound properties from Table 1
- Element type: 3D solid (C3D8R equivalent), 8-node linear brick with reduced integration
- Mesh: ≈82 000 elements; 5 mm nominal at interface surfaces, 15 mm in module body
- Contact: hard normal contact, Coulomb friction ($\mu = 0.65$) at joints

Mesh convergence was verified across three refinement levels (interface element sizes of 15 mm, 10 mm, and 5 mm). Peak bearing stress changed by less than 3% between the 10 mm and 5 mm meshes, confirming adequate convergence at the adopted density.

6.2 Results

Table 2. FEA results for the reference wall assembly.

Performance Metric	Target	Result	Status
$\sigma_{\max}/\sigma_{\text{mean}}$ at bearing pads	≤ 1.35	1.28	Pass
$\sigma_{\max}/f_{c,d}$ utilization ratio	≤ 0.45	0.31	Pass
V_{Rd}/V_{Ed} shear capacity ratio	≥ 1.50	1.52	Pass
Angular misalignment tolerance	report	$\leq 0.3°$	—
Peak stress location	report	V-groove root	—
Governing failure mode	report	Key root shear	—

Design compressive strength is derived as $f_{c,d} = f_{c,k}/\gamma_M$, with $\gamma_M = 2.0$ adopted as a conservative masonry partial factor per EN 1996-1-1 §2.4.3.

6.3 Sensitivity to Machining Deviation

Parametric studies varied angular misalignment from 0° to 0.5° in 0.1° increments. Results are shown in Figure 7.

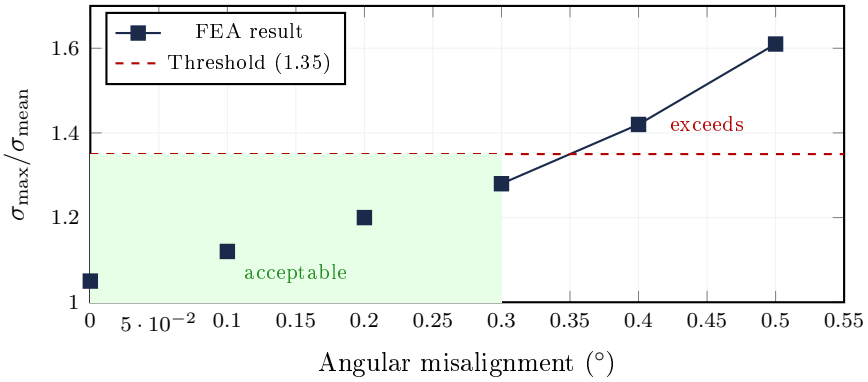

Figure 7. Stress concentration ratio vs. angular misalignment at seating interface. The system remains within the 1.35 threshold up to 0.3°, establishing this as the practical tolerance limit.

Limitation: These results assume linear elastic behavior and perfect contact at datum surfaces. Experimental validation is required before design values can be adopted. The FEA model should be considered a *performance target*, not a validated design basis.

7 Assembly Protocol

Assembly proceeds bottom-up, course-by-course, in running bond. The placement sequence for each module:

1. **Position.** Crane positions module above target location using UID-matched coordinates from the assembly model.
2. **Guide.** Module is lowered into lead-in chamfer engagement zone (±5 mm envelope).
3. **Seat.** Kinematic constraint engages: V-groove locates, datum pads bear, tertiary stop arrests.
4. **Verify.** Seating confirmed by flush-mounted tell-tale pin or digital inclinometer ($\leq 0.1°$ resolution).
5. **Dowel.** Dowels inserted through pre-aligned sockets; grout injected.
6. **Bed.** Bedding mortar (if specified) verified for squeeze-out at joint perimeter.
7. **Log.** Module UID and as-placed survey data logged to assembly model.

Sub-cassette pre-assembly. For façade applications, 2–6 modules may be pre-assembled in workshop conditions, reducing on-site crane operations by approximately 60–70%.

8 Manufacturing Cell Configuration

8.1 Equipment

Table 3. Reference manufacturing cell specification.

Component	Specification
Robotic arm	6-axis, payload $\geq 200\,\text{kg}$, repeatability $\pm 0.05\,\text{mm}$
Spindle	15–25 kW electrospindle, 1000–12000 RPM, HSK-A63, through-tool coolant
Tool changer	≥ 8 positions: roughing discs, finishing profilers, core drills, engraving bits
Fixturing	Vacuum chuck with 3-point kinematic datum, positional accuracy $\pm 0.1\,\text{mm}$
Metrology	Structured-light scanner, point spacing $\leq 0.5\,\text{mm}$, accuracy $\pm 0.05\,\text{mm}$
Dust/slurry	Wet-cutting with closed-loop water recycling

8.2 Dimensional Control Targets

Table 4. Dimensional control targets by surface domain.

Surface Domain	Tolerance	Verification
Interface surfaces (datum, V-groove)	$\pm 0.5\,\text{mm}$	Structured-light scan
Expressive surfaces	$\pm 1.5\,\text{mm}$	Structured-light scan
Shear key depth	$\pm 0.3\,\text{mm}$	Structured-light scan
Dowel hole position	$\leq 1.0\,\text{mm}$ positional	Touch probe
Dowel hole diameter	$+1.0/-0.0\,\text{mm}$	Go/no-go gauge
UID engraving	Legible at 0.5 m	Visual inspection

9 Lifecycle and Embodied Carbon (Preliminary)

9.1 System Boundary

The lifecycle scope is cradle-to-grave per EN 15978: modules A1–A5 (production and construction), B1–B5 (use-phase maintenance), C1–C4 (end-of-life). Module D (reuse potential) reported separately. Functional unit: $1\,\text{m}^2$ of structural wall providing equivalent capacity ($\geq 500\,\text{kN/m}$ compression, $\geq 75\,\text{kN/m}$ shear) over the specified service life.

9.2 Indicative Comparison

Table 5. Indicative lifecycle comparison (pending full LCA).

Parameter	Modular Stone	Precast Concrete	Unit
Embodied carbon (A1–A3)	40–55*	80–180	$\text{kgCO}_2\text{e/m}^2$
Design service life	100–200+	40–60	years
Annualized carbon	0.20–0.55	1.3–4.5	$\text{kgCO}_2\text{e/m}^2\text{/yr}$
End-of-life reuse potential	High	Low–Medium	—
Maintenance interval	50–100	15–30	years

*Baseline: French limestone, quarry distance $\leq$100 km, robotic machining at 8–12 kWh/m^3.

The annualized carbon comparison is the strongest argument for stone's lifecycle performance. The narrowed range for modular stone (40–55 $\text{kgCO}_2\text{e/m}^2$) assumes a baseline scenario: European limestone quarry within 100 km transport distance, robotic machining energy intensity

of 8–12 kWh/m^3 (measured at comparable CNC stone facilities), 0.4 m wall thickness, and a grid carbon intensity of 0.25 kgCO_2e/kWh (approximate EU-27 2024 average). The primary drivers of variance are transport distance, stone density, and local grid mix; granite assemblies at longer distances or in coal-dependent grids would shift toward the upper bound. A full LCA with primary energy data from instrumented fabrication cells is required before publication-grade claims can be made.

10 Research Agenda

10.1 Phase 1: Experimental Validation (Year 1)

1. **Joint testing.** Fabricate ≥ 12 joint specimens per interface class under monotonic compression, shear, and combined loading. Deliverable: characteristic strength values. Target: CoV $\leq 15\%$.
2. **Tolerance sensitivity.** Fabricate joints with controlled misalignments (0–0.5° angular, 0–1.5 mm positional) and test to failure. Deliverable: validated failure envelope. Target: FEA correlation ≥ 0.85.
3. **Bedding creep.** Long-duration ($\geq$ 6 month) creep testing of thin-bed mortar under sustained compression. Deliverable: creep coefficient vs. time.

10.2 Phase 2: System-Level Testing (Year 2)

4. **Wall demonstrator.** Construct a full-scale wall (≥ 48 modules) and test under vertical load and cyclic lateral loading. Deliverable: load-displacement curves, failure documentation. Target: lateral capacity $\geq 1.5\times$ design.
5. **Long-term monitoring.** Instrument demonstrator with strain gauges and displacement transducers for $\geq$ 12-month monitoring.

10.3 Phase 3: Comparative Assessment (Years 2–3)

6. **Full LCA.** Cradle-to-grave per EN 15978 with primary data. Deliverable: EPD-quality dataset.
7. **Economic modeling.** Parametric cost comparison vs. precast concrete and GFRC at 500–10,000 m^2 project scales.
8. **Discrete element validation.** Compare FEA results with DEM modeling for non-linear joint behavior and progressive failure.

11 Governance and Versioning

MSS-RSC is released as:

- A versioned, open academic protocol under CC-BY-SA 4.0
- A non-commercial research artefact intended for replication and critique
- A living document; future versions will incorporate experimental data, revised safety factors, and community-contributed extensions

Version history:

- **Initial Public Release** (Feb 2026): Interface taxonomy with four specified classes, digital-to-physical workflow, preliminary FEA validation, material properties, assembly protocol, normative requirements, and TikZ technical diagrams. Released as open academic protocol for replication and critique.

12 Conclusion

MSS-RSC defines a mechanical interface protocol enabling deterministic modular stone construction under robotic fabrication constraints. The protocol specifies four interface classes—kinematic seating, shear-transfer keys, dowel indexing, and controlled bedding—each with dimensional tolerances, performance equations, and verification procedures. These are integrated within a digital-to-physical workflow that tracks tolerance from machining through assembly.

The protocol's central contribution is a formalized separation between expressive architectural geometry and invariant structural interfaces, stated as normative requirements. Preliminary finite element analysis bounds the performance envelope: stress uniformity within 8% at bearing interfaces, shear capacity at 1.52× design load, and angular tolerance to 0.3°.

This document does not prescribe architectural form. It prescribes mechanical grammar.

If validated through the experimental program of §10, MSS-RSC may enable structural stone to re-emerge as a scalable, durable, and carbon-efficient construction system.

Nomenclature

Symbol	Definition
σ_{bearing}	Bearing stress at kinematic seating interface (MPa)
$\sigma_{\max}$	Peak bearing stress (MPa)
σ_{mean}	Mean bearing stress (MPa)
F_z	Vertical load (kN)
A_{eff}	Effective bearing area (mm^2)
$f_{c,k}$	Characteristic compressive strength (MPa)
$f_{c,d}$	Design compressive strength (MPa)
γ_M	Material partial safety factor
V_{Rd}	Design shear resistance (kN)
V_{Ed}	Design shear force (kN)
n_k	Number of active shear keys
A_k	Shear key cross-sectional area (mm^2)
f_{vk0}	Characteristic initial shear strength (MPa)
μ	Friction coefficient (dressed stone)
N_{Ed}	Design compressive force on joint (kN)
ϕ	Dowel diameter (mm)
L_{embed}	Dowel embedment length (mm)
f_{bond}	Bond strength, grout-to-stone (MPa)
d_k, w_k	Shear key depth and width (mm)
$r_{\text{eff}}(t)$	Effective tool radius at cutting time t (mm)
α	Tool wear rate (mm/hr) or thermal expansion coefficient
Δz_n	Cumulative vertical deviation at course n (mm)
σ_{mach}	Std. deviation of machining error (mm)
E_{bed}	Bedding mortar elastic modulus (GPa)
φ	Creep coefficient (bedding mortar)

References

[1] J. Heyman, *The Stone Skeleton: Structural Engineering of Masonry Architecture*, Cambridge University Press, 1995.

[2] J. Ochsendorf, "Collapse of Masonry Structures," Ph.D. dissertation, University of Cambridge, 2002.

[3] T. Bonwetsch, F. Gramazio, M. Kohler, "The Informed Wall: Applying Additive Digital Fabrication Techniques on Architecture," *Proc. ACADIA*, 2006.

[4] T. Sandy et al., "Autonomous repositioning and localization of an in situ fabricator," *IEEE Int. Conf. Robotics and Automation*, 2016.

[5] G. Fallacara, "Toward a Stereotomic Design: Experimental Constructions and Didactic Experiences," *Proc. Third Int. Congress on Construction History*, 2009.

[6] P. Block, J. Ochsendorf, "Thrust Network Analysis: A New Methodology for Three-Dimensional Equilibrium," *J. Int. Assoc. Shell and Spatial Structures*, vol. 48, no. 3, 2007.

[7] M. Rippmann, T. Van Mele, P. Block, "The Armadillo Vault: Computational Design and Digital Fabrication of a Freeform Stone Shell," *Advances in Architectural Geometry*, 2016.

[8] E.M. Winkler, *Stone in Architecture: Properties, Durability*, 3rd ed., Springer, 1994.

[9] EN 1996-1-1:2005+A1:2012, *Eurocode 6: Design of Masonry Structures*, European Committee for Standardization.

[10] EN 1991-1-4:2005, *Eurocode 1: Actions on Structures — Wind Actions*, European Committee for Standardization.

[11] EN 15978:2011, *Sustainability of Construction Works — Assessment of Environmental Performance of Buildings*, European Committee for Standardization.